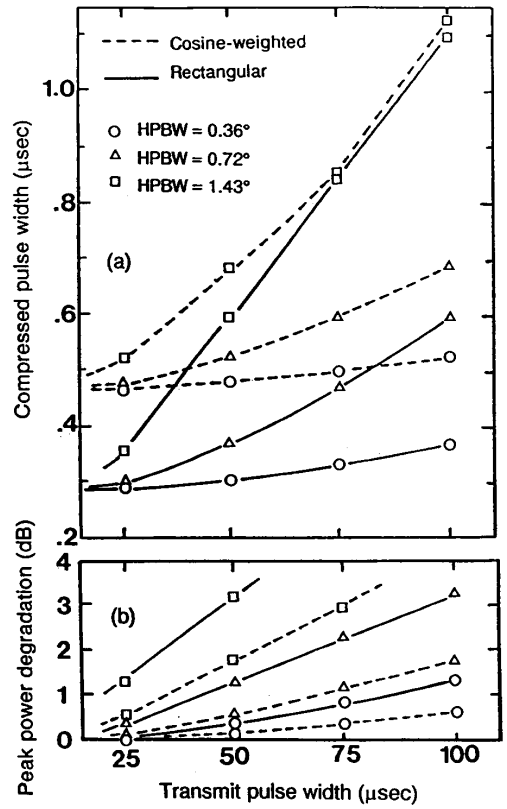

Fig. 4. Compressed pulse width p_w (a) and the degradation in compressed peak power ΔP (b) as a function of T_W for several antenna beam widths. Notation of lines and symbols in (a) also applies to (b).

return signal clearly affects range resolution and the peak power level of a compressed pulse. This means that the "effective" compression ratio is degraded by signal decorrelation. It is also found that the sidelobe shape is modified by the decorrelation (i.e., sidelobe nulls entirely disappear) and that the sidelobe levels averaged over a sidelobe "cycle" (from null to null) are not affected by signal decorrelation. The latter fact suggests that signal decorrelation does not degrade the ratio of rain echo to the range sidelobe interference level, because the rain echo level is approximately proportional to the product of compressed pulse width and the compressed peak power which is found to be almost constant regardless of signal decorrelation from the numerical calculation.

The compressed pulse width (p_w; −3-dB width) and the decrease in compressed peak power (ΔP in decibel) obtained from each calculated waveform are shown in Fig. 4 as a function of transmit pulse width T_W. As a guideline of the limit of T_w that gives tolerable degradation in pulse compression performance, we consider T_w values at which p_w and ΔP are degraded by 10 and 20% (in the case of ΔP, 0.45 and 0.97 dB). Those T_w values are estimated from second-order polynomial regressions of the curves shown in Fig. 4, and the following results are obtained:

1) To keep the degradations in p_w and ΔP within 10% (0.45 dB), T_W should be less than $0.56\tau_{0.1}$ for the rectangular pulse, and $0.86\tau_{0.1}$ for the cosine pulse;

2) To keep the degradations in p_w and ΔP within 20% (0.97 dB), T_W should be less than about $0.8\tau_{0.1}$ for the rectangular pulse, and about $1.3\tau_{0.1}$ for the cosine pulse.

It should be noted that the results shown in Figs. 2–4 are based on the calculation using (14), which neglects the delay time difference between the center and the edge of the FOV. If this time difference cannot be omitted, the compressed waveform may not be symmetrical with respect to the mainlobe. In general, the trailing sidelobe is more affected by the signal decorrelation than is the leading sidelobe, because the return from the edge of the FOV decorrelates more quickly than that from the center of the FOV. In such cases, the reuslts shown here should be understood as an "average" of the leading and the trailing sidelobes. It has been found from the rigorous calculation of (12) that the sidelobes for antenna beamwidths up to 0.72° are approximately symmetric with respect to the mainlobe peak.

V. Summary

We have considered an inherent problem in pulse-compression radar systems used for nadir-looking spaceborne radars. As anticipated, if the transmitted pulse width (T_W) becomes longer than the signal decorrelation time, the effective compression ratio (range resolution and compressed peak power) is significantly degraded; however, "absolute" sidelobe levels are approximately constant. The effects of signal decorrelation somewhat depend on the particular waveform. Generally speaking, the stronger the time or frequency domain weighting to obtain low range sidelobe levels, the less the effects of signal decorrelation. Judging from the results shown above, however, we can conclude that T_W should be shorter than about half the $\tau_{0.1}$ (the time for $\rho(\tau)$ to decrease to 0.1) so that the signal decorrelation effects are negligible.

References

[1] T. Manabe and T. Ihara, "A feasibility study of rain radar for the Tropical Rainfall Measuring Mission, 5. Effects of surface clutter on rain measurements from space," *J. Commun. Res. Lab.*, vol. 35, no. 145, pp. 163–181, 1988.

[2] R. W. Gray and D. T. Farley, "Theory of incoherent-scatter measurements using compressed pulses," *Radio Sci.*, vol. 8, no. 2, pp. 123–131, 1973.

[3] K. Wakasugi, M. Matsuo, S. Fukao, and S. Kato, "Pulse-compression technique for radar observations of the middle atmosphere," *Trans. IECE, Japan*, vol. J65-B, no. 10, pp. 1260–1266, 1982 (in Japanese).

[4] R. Meneghini and T. Kozu, *Spaceborne Weather Radar*, Chap. 2. Norwood, MA: Artech House, 1990.

[5] K. Okamoto, J. Awaka, and T. Kozu, "A feasibility study of rain radar for the Tropical Rainfall Measuring Mission, 6. A case study of rain radar system," *J. Commun. Res. Lab.*, vol. 35, no. 145, pp. 183–208, 1988.

Maximum-Likelihood Blind Deconvolution: Non-White Bernoulli–Gaussian Case

Chong-Yung Chi and Wu-Ton Chen

***Abstract*—Todoeschuck and Jensen [1], [2] recently reported that some reflectivity sequences $\mu(k)$ calculated from sonic logs are not white**

Manuscript received February 11, 1991. This work was supported by National Science Council Grant NSC80-0404-E-007-27.

C-Y. Chi and W-T. Chen are with the Department of Electrical Engineering, National Tsing Hua University, Hsinchu, Taiwan 30043, Republic of China.

IEEE Log Number 9101246.

and have a power spectral density approximately proportional to frequency, called a Joseph spectrum. The well-known MLD algorithms [7]–[13] can simultaneously provide estimates of $\mu(k)$, source wavelet which need not be minimum-phase, and statistical parameters. Although these MLD algorithms work well, they are based on the white Bernoulli–Gaussian (B-G) model for $\mu(k)$. In this paper, assuming that spectrum measurements of $\mu(k)$ are available, we propose a ML algorithm for blind deconvolution as $\mu(k)$ is nonwhite with a general spectrum meanwhile the spectrum of the obtained maximum-likelihood estimate $\hat{\mu}_{ML}(k)$ is consistent with the measured spectrum.

I. Introduction

The estimation of the desired signal $\mu(k)$ from noisy measurements $z(k)$, $k = 1, 2, \cdots, N$, obtained from the following convolutional model

$$z(k) = \mu(k) * v(k) + n(k) = \sum_{i=0}^{k} v(i)\mu(k-i) + n(k) \quad (1)$$

where $v(k)$ is the impulse response of a linear time-invariant system and $n(k)$ is the measurement noise, is a deconvolution problem. This problem can be found in areas such as seismology, astronomy, speech processing, biomedical ultrasonic imaging, and communications. Conventionally, the *whiteness* assumption about $\mu(k)$ is used in seismic deconvolution such as predictive deconvolution [3]–[4], minimum-variance deconvolution (MVD) [5]–[6] and maximum-likelihood deconvolution (MLD) [7]–[13].

Todoeschuck and Jensen [1] recently reported that some reflectivity sequences $\mu(k)$, calculated from sonic logs are not white and have a power spectral density approximately proportional to frequency, called a Joseph spectrum. In view of this fact, Chi [14], [15] modeled $\mu(k)$, whose spectrum is Joseph, as the output of a minimum-phase coloring filter $v_1(k) = \delta(k) - 0.51\delta(k-1)$ that is excited by white Bernoulli–Gaussian (B-G) process $\xi(k)$ as follows:

$$\mu(k) = \xi(k) * v_1(k) \quad (2)$$

where

$$\xi(k) = r(k) \cdot q(k) \quad (3)$$

$r(k)$ is zero-mean white Gaussian with variance σ_r^2 and $q(k)$ is Bernoulli for which

$$P_r[q(k)] = \begin{cases} \lambda, & q(k) = 1 \\ 1 - \lambda, & q(k) = 0. \end{cases} \quad (4)$$

He then showed how to obtain minimum-variance estimate $\hat{\mu}_{MV}(k)$ and maximum-likelihood estimate $\hat{\mu}_{ML}(k)$ of $\mu(k)$ assuming that coloring filter $v_1(k)$, source wavelet $v(k)$, and all statistical parameters (σ_r^2, λ and variance σ_n^2 of white noise $n(k)$) are given in advance.

In practice, not only $\mu(k)$ but also $v(k)$ and statistical parameters must be estimated from data $z(k)$. It is so called blind deconvolution. The well-known MLD algorithms [7]–[9], which are based on the white B-G model for $\mu(k)$, can simultaneously provide estimates of $\mu(k)$, $v(k)$ which need not be minimum-phase, and statistical parameters. However, maximum-likelihood blind deconvolution for the case that $\mu(k)$ has a general spectrum is still an unknown problem. On the other hand, the spectrum of $\mu(k)$ calculated from sonic logs, may be available in the meantime. It is clearly better [1] to deconvolve seismograms meanwhile taking the spectrum of $\mu(k)$ into account if it has been calculated from sonic logs.

In this paper, we propose a ML algorithm for blind deconvolution as $\mu(k)$ is nonwhite with a general spectrum meanwhile the spectrum of ML estimate $\hat{\mu}_{ML}(k)$ is consistent with the measured spectrum. In Section II, we present the MLD of nonwhite B-G signals. Then, we show some simulation results to demonstrate the good performance of the proposed ML blind deconvolution algorithm for nonwhite B-G signals in Section III. Finally, we draw some conclusions.

II. MLD of Non-White B-G Signals

The proposed MLD algorithm is, again, based on the model (2) and (3) for $\mu(k)$ where $v_1(k)$, now, is the impulse response of an unknown causal stable linear time-invariant system and it can be nonminimum-phase. Assume that $V_1(z)$ (z-transform of $v_1(k)$) and $V(z)$ are rational functions and that pole-zero cancellation does not occur in $V_1(z) \cdot V(z)$, denoted $V_2(z)$, which is the z-transform of the combined wavelet $v_2(k)$ where

$$v_2(k) = v_1(k) * v(k). \quad (5)$$

The algorithm to be presented consists of two parts. One part includes estimation of $\xi(k)$ and $v_2(k)$ from $z(k)$. The other part includes estimation of $\mu(k)$ and $v_1(k)$ from the estimates $\hat{\xi}_{ML}(k)$ and $\hat{v}_2(k)$, and the measured spectrum of $\mu(k)$. Next, let us present the former and then the latter, respectively.

A. Estimation of $\xi(k)$ and $v_2(k)$

From (1) and (2) we have

$$z(k) = \xi(k) * v_2(k) + n(k). \quad (6)$$

Note, from (6), that $z(k)$ can be viewed as the output of a linear causal stable time-invariant system $v_2(k)$ with input being a white B-G signal $\xi(k)$. The well-known MLD algorithm [9], which is based on the maximization of the following likelihood function

$$S\{\underline{r}, \underline{q}, \underline{\theta}, \lambda, \sigma_n^2 | \underline{z}\} = p(\underline{z}, \underline{r}, \underline{q} | \underline{\theta}, \lambda, \sigma_n^2, \sigma_r^2) \quad (7)$$

where $\underline{z} = (z(1), z(2), \cdots, z(N))'$, $\underline{r} = (r(1), r(2), \cdots, r(N))'$, $\underline{q} = (q(1), q(2), \cdots, q(N))'$ and $\underline{\theta}$ contains all the coefficients of $V_2(z)$, includes estimation of $v_2(k)$, detection of $q(k)$, estimation of $r(k)$ and estimation of statistical parameters λ, σ_n^2. The parameter σ_r^2 is never estimated due to a scale factor existing between $v_2(k)$ and $\xi(k)$. Their MLD algorithm has been successfully used to process real seismic data. Surely, we can obtain ML estimates, $\hat{V}_2(z)$ and $\hat{\xi}_{ML}(k) = \hat{r}_{ML}(k) \cdot \hat{q}_{ML}(k)$ by use of their MLD algorithm. The reader can refer to [9] for details of their MLD algorithm.

B. Estimation of $\mu(k)$ and $v_1(k)$

It is well known that the ML estimate of $\mu(k)$ can be computed by

$$\hat{\mu}_{ML}(k) = \hat{\xi}_{ML}(k) * v_1(k) \quad (8)$$

which is, however, not computable since $v_1(k)$ is not known. In other words, the MLD algorithm is not able to provide $\hat{\mu}_{ML}(k)$ unless $v_1(k)$ can be estimated via some extra information (such as spectrum or autocorrelation function of $\mu(k)$ calculated from sonic logs) other than data $z(k)$. Next, let us present the algorithm for finding the optimum $\hat{V}_1(z)$ from $\hat{V}_2(z)$ such that the associated normalized autocorrelation function (see (9) below) of $\hat{\mu}_{ML}(k)$ is consistent with the measured normalized autocorrelation function of $\mu(k)$ under the constraint that $\hat{V}_2(z) = \hat{V}_1(z) \cdot \hat{V}(z)$.

Let $r_\mu(k)$ denote the normalized autocorrelation function of $\mu(k)$, defined as

$$r_\mu(k) = \frac{\sum_{i=1}^{N} \mu(i)\mu(i+k)}{\sum_{i=1}^{N} \mu^2(i)}. \quad (9)$$

Note that $r_\mu(0) = 1$ for any $\mu(k)$. Assume that $\bar{r}_\mu(k)$ is the measured normalized autocorrelation function of $\mu(k)$. The optimum $v_1(k)$ is the one such that the following sum of error squares:

$$J(\hat{V}_1(z)) = \sum_{k=1}^{M} |\hat{r}_\mu(k) - \bar{r}_\mu(k)|^2 \tag{10}$$

is minimum where M denotes the length of $\bar{r}_\mu(k)$ and $\hat{r}_\mu(k)$ is computed by (8) and (9) with $v_1(k) = \hat{v}_1(k)$.

We express the rational transfer function $\hat{V}_2(z)$ as

$$\hat{V}_2(z) = \beta \frac{Q(z)}{P(z)} \tag{11}$$

where β is a nonzero constant

$$P(z) = \prod_{i=1}^{m_1} P_i(z) \cdot \prod_{i=m_1+1}^{m_2} P_i(z) \tag{12}$$

$$Q(z) = \prod_{i=1}^{n_1} Q_i(z) \cdot \prod_{i=n_1+1}^{n_2} Q_i(z) \tag{13}$$

$$P_i(z) = \begin{cases} 1 - p_i z^{-1}, & 1 \le i \le m_1 \text{ and real } p_i \\ (1 - p_i z^{-1})(1 - p_i^* z^{-1}), & \\ & m_1 + 1 \le i \le m_2 \text{ and complex } p_i \end{cases} \tag{14}$$

$$Q_i(z) = \begin{cases} 1 - q_i z^{-1}, & 1 \le i \le n_1 \text{ and real } q_i \\ (1 - q_i z^{-1})(1 - q_i^* z^{-1}), & \\ & n_1 + 1 \le i \le n_2 \text{ and complex } q_i \end{cases} \tag{15}$$

m_1 and n_1 denote the number of real roots of $P(z)$ and $Q(z)$, respectively, $(m_2 - m_1)$ and $(n_2 - n_1)$ denote the number of pairs of complex conjugate roots of $P(z)$ and $Q(z)$, respectively. Since $\hat{V}_1(z)$ is a factor of $\hat{V}_2(z)$ due to $\hat{V}_2(z) = \hat{V}_1(z) \cdot \hat{V}(z)$, there exist 2^L possible $\hat{V}_1(z)$'s, where $L = m_2 + n_2$. Therefore, the computational load of searching for the optimum $\hat{V}_1(z)$ from 2^L possible candidates could be heavy when 2^L is large.

In view of the possible heavy computational load, we propose an iterative fast search algorithm, which is shown in Fig. 1, for the desired $\hat{V}_1(z)$. Let $b_i(k)$ be a binary sequence for which either $b_i(k) = 0$ or $b_i(k) = 1$, for all $1 \le k \le L$. Assume that at the $(i-1)$th iteration we ended up with $\hat{V}_{1,i-1}(z)$ where

$$\hat{V}_{1,i-1}(z) = \frac{\prod_{k=1}^{n_2} [Q_k(z)]^{b_{i-1}(k)}}{\prod_{k=n_2+1}^{L} [P_{k-n_2}(z)]^{b_{i-1}(k)}}. \tag{16}$$

For the ith iteration, the algorithm computes L objective functions $J(V_1^j(z)), j = 1, 2, \cdots, L$, where $V_1^j(z)$ is defined as

$$V_1^j(z) = \frac{\prod_{k=1}^{n_2} [Q_k(z)]^{b_j'(k)}}{\prod_{k=n_2+1}^{L} [P_{k-n_2}(z)]^{b_j'(k)}} \tag{17}$$

where

$$b_j'(k) = \begin{cases} b_{i-1}(k), & k \ne j \\ 1 - b_{i-1}(k), & k = j. \end{cases} \tag{18}$$

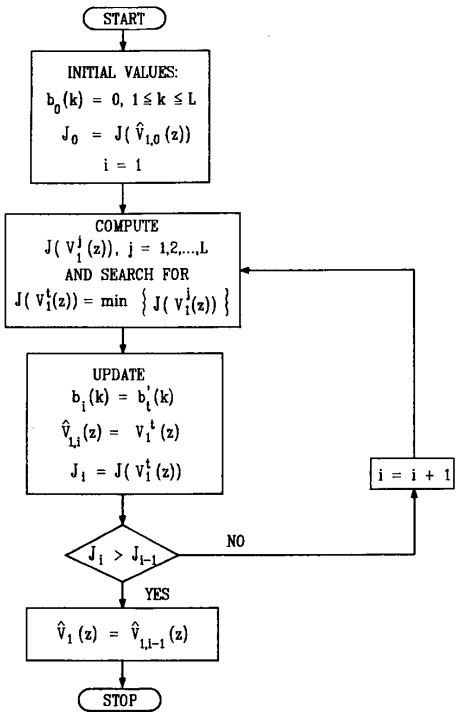

Fig. 1. Fast search algorithm for $\hat{V}_1(z)$.

Note, from (16) through (18), that $V_1^j(z)$ differs from $\hat{V}_{1,i-1}(z)$ only in either a factor $Q'(z) \in \{Q_k(z),\ 1 \le k \le n_2\}$ for $1 \le j \le n_2$ in the numerator or a factor $P'(z) \in \{P_k(z),\ 1 \le k \le m_2\}$ for $n_2 + 1 \le j \le L$ in the denominator. Then we search for the minimum over $\{J(V_1^j(z)),\ 1 \le j \le L\}$, denoted by $J(V_1^t(z))$, i.e.,

$$J(V_1^t(z)) = \min \{J(V_1^j(z))\}. \tag{19}$$

Finally, $b_i(k)$, $\hat{V}_{1,i}(z)$ and J_i are updated as follows:

$$b_i(k) = b_t'(k) \tag{20}$$

$$\hat{V}_{1,i}(z) = V_1^t(z) \tag{21}$$

$$J_i = J(V_1^t(z)). \tag{22}$$

When $J_i > J_{i-1}$ the algorithm converges, we obtain $\hat{V}_1(z) = \hat{V}_{1,i-1}(z)$ and $\hat{V}(z) = \hat{V}_2(z)/\hat{V}_1(z)$. The fact that the algorithm is fast is based on: (1) the objective function J is guaranteed to decrease for every iteration; and (2) the algorithm converges in less than or equal to L iterations.

As a final remark, a scale factor associated with $\hat{V}_1(z)$ and $\hat{V}(z)$ is not resolvable since for any nonzero constant α, $(\alpha \hat{V}_1(z), \hat{V}(z)/\alpha)$ and $(\hat{V}_1(z), \hat{V}(z))$ lead to $\hat{\mu}_{ML}(k)$'s with the same normalized autocorrelation function. Next, we present some simulation results to demonstrate that the proposed MLD algorithm works well.

III. Computer Simulation

For our simulation a pseudo white B-G signal $\xi(k)$ was generated and then convolved with

$$v_1(k) = \delta(k) - 1.9660\delta(k-1) \tag{23}$$

which is maximum-phase, to obtain true $\mu(k)$ which has a Joseph

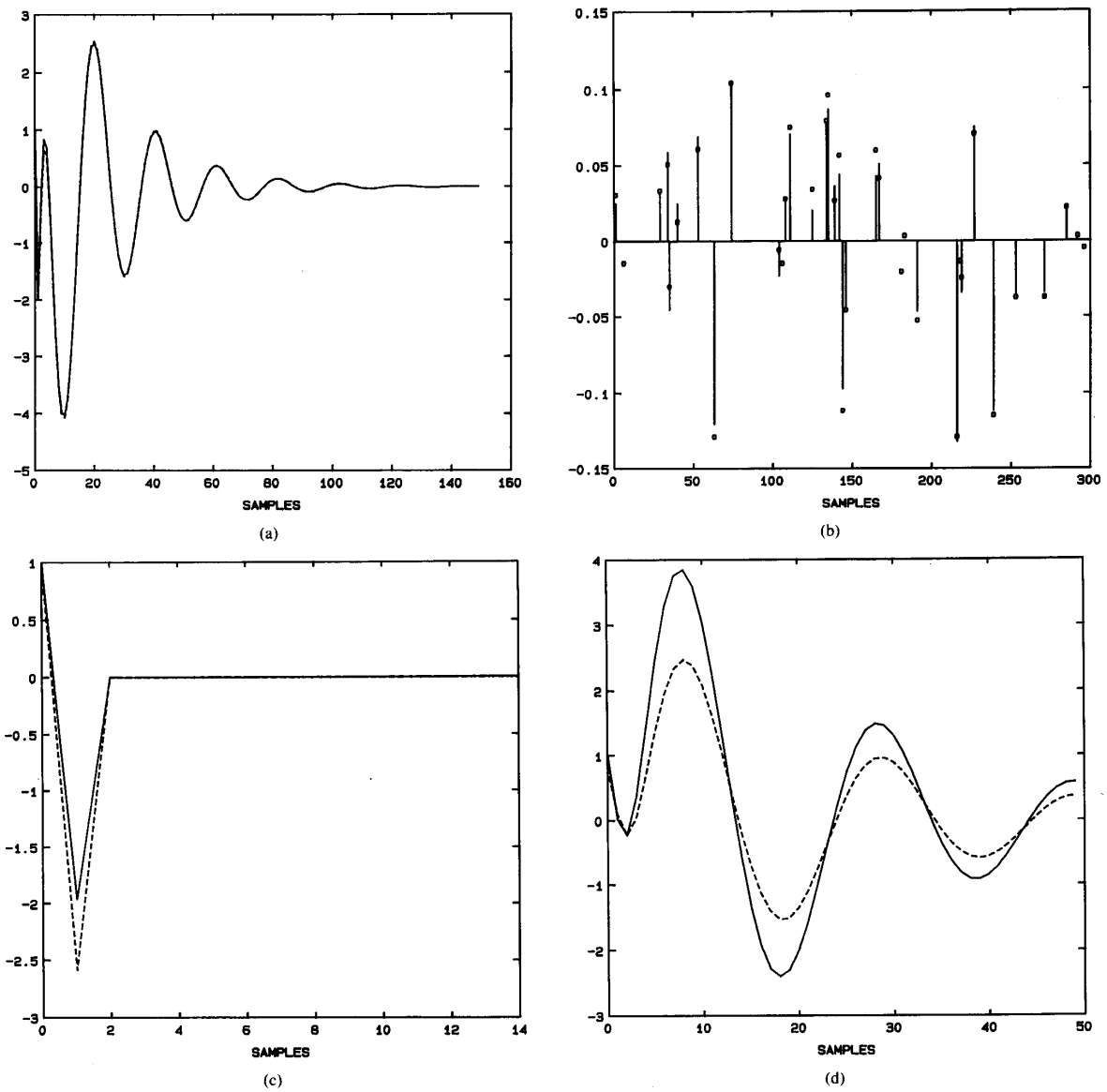

Fig. 2. (a) The combined source wavelet $v_2(k)$ (solid line) and estimate $\hat{v}_2(k)$ (dashed line); (b) $\xi(k)$ (circles) and $\hat{\xi}_{ML}(k)$ (bars); (c) $v_1(k)$ (solid line) and estimate $\hat{v}_1(k)$ (dashed line); (d) source wavelet $v(k)$ (solid line) and estimate $\hat{v}(k)$ (dashed line); (e) normalized autocorrelation functions $\hat{r}_\mu(k)$ (dashed line) and $\bar{r}_\mu(k)$ (solid line); and (f) $\mu(k)$ (top part) and $\hat{\mu}_{ML}(k)$ (bottom part).

spectrum. The simulated $z(k)$, $k = 1, 2, \cdots, N = 300$, were obtained by convolving $\mu(k)$ with the nonminimum-phase source wavelet $v(k)$, whose transfer function is given by

$$V(z) = \frac{1 - 2.5654z^{-1} + 2.1996z^{-2}}{1 - 2.5860z^{-1} + 2.4890z^{-2} - 1.033z^{-3} + 0.1680z^{-4}} \tag{24}$$

to obtain the noise-free data and then adding white Gaussian noise to the noise-free data with signal-to-noise ratio (SNR) equal to 15. On the other hand, the simulated normalized autocorrelation function $\bar{r}_\mu(k)$ was calculated by (9) with $\mu(k) = \bar{\mu}(k)$ where $\bar{\mu}(k)$ was obtained by adding white Gaussian noise to $\mu(k)$ with SNR = 15. The true $V_2(z)$ $(= V_1(z) \cdot V(z))$ is, therefore, a fourth-order rational function as follows:

$$V_2(z) = \frac{1 - 4.5314z^{-1} + 7.2431z^{-2} - 4.3244z^{-3}}{1 - 2.5860z^{-1} + 2.4890z^{-2} - 1.033z^{-3} + 0.1680z^{-4}}. \tag{25}$$

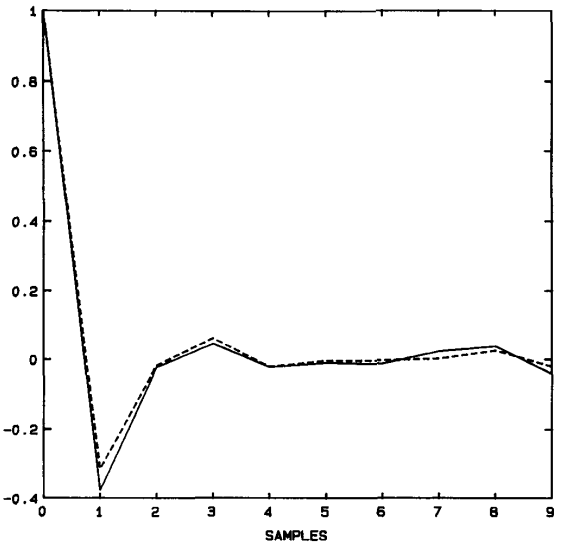

(e)

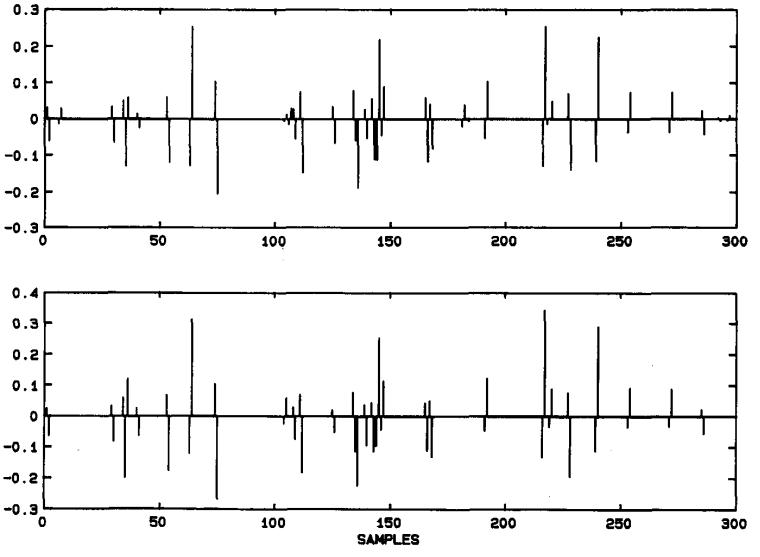

(f)

Fig. 2. (*Continued*)

The order of $\hat{V}_2(z)$ used was equal to 4. We then obtained $\hat{\xi}_{ML}(k)$ and $\hat{V}_2(z)$ using Chi, Mendel, and Hampson's MLD algorithm [9]. Finally, we obtained $\hat{\mu}_{ML}(k)$, $\hat{V}_1(z)$ and $\hat{V}(z)$ by the algorithm described in Section II with the parameter $M = 9$ (length of $\bar{r}_\mu(k)$).

The simulation results are shown in Fig. 2. The obtained $\hat{V}_2(z)$ is given as follows:

$$\hat{V}_2(z) = \frac{0.8039 - 4.1008z^{-1} + 6.8305z^{-2} - 4.1489z^{-3}}{1 - 2.6297z^{-1} + 2.5908z^{-2} - 1.1136z^{-3} + 0.1885z^{-4}}. \tag{26}$$

The combined source wavelet $v_2(k)$ (solid line) and estimate $\hat{v}_2(k)$ (dashed line) are shown in Fig. 2(a) from which one can see that $\hat{v}_2(k)$ is a good approximation to $v_2(k)$, although the coefficients of $\hat{V}_2(z)$ are different from those of $V_2(z)$. $\hat{\xi}_{ML}(k)$ (bars) and $\xi(k)$ (circles) are depicted in Fig. 2(b), where the former is also a good approximation to the latter. $v_1(k)$ (solid line) and estimate $\hat{v}_1(k)$ (dashed line) are shown in Fig. 2(c), from which one can see that $\hat{v}_1(k)$ is also maximum-phase. From Fig. 2(d), we see that the estimate $\hat{v}(k)$ (dashed line) is also a good approximation to the wavelet $v(k)$ (solid line). Note that the scale factor associated with $\hat{v}_1(k)$ and $\hat{v}(k)$ was not existent due to $\hat{v}_1(0) = v_1(0) = 1$ for this case. The normalized autocorrelation function $\hat{r}_\mu(k)$ (dashed line) of $\hat{\mu}_{ML}(k)$ and $\bar{r}_\mu(k)$ (solid line) are shown in Fig. 2(e) which implies the consistency of spectrum of $\hat{\mu}_{ML}(k)$ with that of $\tilde{\mu}(k)$. Finally, true $\mu(k)$ (top part) and $\hat{\mu}_{ML}(k)$ (bottom part) are shown in Fig. 2(f) from which one can observe that $\hat{\mu}_{ML}(k)$ is quite close to $\mu(k)$.

The true order for $\hat{V}_2(z)$ was used in the previous simulation. We also performed the same simulation with the order of $\hat{V}_2(z)$ equal to 5 which is one order higher than that of $V_2(z)$. Very similar results were obtained and thus are omitted here. These simulations also demonstrated that the proposed MLD algorithm performs well as long as the order of $\hat{V}_2(z)$ used is large enough.

IV. Conclusions

In this paper, we have presented a MLD algorithm for estimating nonwhite B-G signals $\mu(k)$, which were distorted by a linear time-invariant system $v(k)$ meanwhile taking into account of the measured spectrum of $\mu(k)$ such as that obtained from sonic logs. Without the information of spectrum of $\mu(k)$, the MLD algorithm can only provide the ML estimate $\hat{\xi}_{ML}(k)$ of white B-G signal $\xi(k)$, which could be very different from $\mu(k) = \xi(k) * v_1(k)$ (see (2)) if the normalized autocorrelation function of $\mu(k)$ is broad (i.e., away from $\delta(k)$). The proposed MLD algorithm can recover both the phase of $v_1(k)$ and that of $v(k)$ as long as the spectrum of $\mu(k)$ is known in advance. We also presented some simulation results which supported the proposed MLD algorithm.

Remark that the proposed algorithm is based on the assumption that pole-zero cancellation does not occur in $V_2(z) = V_1(z) \cdot V(z)$. However, the case that pole-zero cancellation happens, was not considered in this paper. We leave the problem of how to extract $v_1(k)$ for this rare case in the future research.

Acknowledgment

The research described in this paper was performed at the Department of Electrical Engineering, National Tsing Hua University, Hsinchu, Taiwan, Republic of China.

References

[1] J. P. Todoeschuck and O. G. Jensen, "Joseph geology and seismic deconvolution," *Geophysics*, vol. 53, no. 11, pp. 1410-1414, Nov. 1988.

[2] J. P. Todoeschuck, O. G. Jensen, and S. Labonte, "Gaussian scaling noise model of seismic reflection sequences: Evidence from well logs," *Geophysics*, vol. 55, no. 4, pp. 480-484, April 1990.

[3] E. A. Robinson, "Predictive decomposition of seismic traces," *Geophysics*, vol. 22, pp. 767-778, 1957.

[4] E. A. Robinson and S. Treitel, *Geophysical Signal Analysis*. Englewood Cliffs, NJ: Prentice Hall, 1980.

[5] J. M. Mendel, "White noise estimators for seismic data processing in oil exploration," *IEEE Trans. Auto. Control*, vol. AC-22, pp. 694-706, 1977.

[6] J. M. Mendel, "Minimum-variance deconvolution," *IEEE Trans. Geosci. Remote Sensing*, vol. GE-19, no. 3, pp. 161-171, July 1981.

[7] J. Kormylo and J. M. Mendel, "Maximum-likelihood deconvolution," *IEEE Trans. Geosci. Remote Sensing*, vol. GE-21, pp. 72-82, 1983.

[8] J. M. Mendel, *Optimal Seismic Deconvolution: An Estimation-Based Approach*. New York: Academic Press, 1983.

[9] C.-Y. Chi, J. M. Mendel, and D. Hampson, "A computationally-fast approach to maximum-likelihood deconvolution," *Geophysics*, vol. 49, pp. 550-565, May 1984.

[10] J. Goutsias and J. M. Mendel, "Maximum-likelihood deconvolution: An optimization theory perspective," *Geophysics*, vol. 51, no. 6, pp. 1206-1220, 1986.

[11] G. B. Giannakis and J. M. Mendel, "Entropy interpretation of maximum-likelihood deconvolution," *Geophysics*, vol. 52, no. 12, pp. 1621-1630, 1987.

[12] J. M. Mendel, *Maximum-Likelihood Deconvolution: A Journey into Model-Based Signal Processing*. New York: Springer-Verlag, 1990.

[13] C-Y. Chi and W-T. Chen, "An adaptive maximum-likelihood deconvolution algorithm," to appear in *Signal Processing*.

[14] C-Y. Chi, "A robustness test for the MVD filter and the MLD algorithm," *IEEE Trans. Geosci. and Remote Sensing*, vol. 29, no. 2, pp. 340-342, March 1991.

[15] C-Y. Chi, "Minimum-variance deconvolution and maximum-likelihood deconvolution for non-white Bernoulli-Gaussian processes with a Joseph spectrum," to appear in *IEEE Trans. Signal Processing*.

Numerical Simulation of Subsurface Radar for Detecting Buried Pipes

Ce Liu and Liang C. Shen

***Abstract*—A subsurface radar for the detection of dielectric or metal pipes buried in the ground is investigated numerically. The two-dimensional transmission line matrix (TLM) method is used to obtain images of buried pipes illuminated by electromagnetic pulses generated by a ground-penetrating radar.**

I. Introduction

Several subsurface sensing radars have been developed recently for the purpose of detecting underground objects such as pipes, buried wastes, and fractures in rock formations [1]-[6]. These radars use synthetic RF pulses [1], mono-cycle pulses [3], and regular electromagnetic impulses [2], [5], [6]. A physical scale model system for studying these radars is presented in [7]. A study of the propagation of electromagnetic pulses in the dissipative and dispersive earth is given in [8], but the study does not include any underground targets. A theoretical estimate of the propagation velocity and depth of the object is given in [9]. The theory is based on Fresnel or Fraunhoffer approximation. The objective of the present study is to numerically simulate the electromagnetic-pulse radar based on rigorous Maxwell's equations. The simulation is aimed at improving the design of the radar and the quality of the images it produces.

Simulation of the electromagnetic-pulse ground-penetrating radar is accomplished by using the transmission-line-matrix (TLM) method. This method has been used widely in solving microwave problems which involve finite regions bounded by conductors, such as waveguides or resonant cavities. A summary paper on TLM technique is given by Hoefer [10]. The TLM method has been successfully used in solving a well-logging problem involving open regions [11]. It has been shown that by judiciously choosing artificial boundaries and by applying the so-called absorbing boundary condition, the TLM technique can also solve many open-boundary problems in the time domain. While the well-logging problem studied in [11] is a two-dimensional one in the cylindrical coordinate system, the present problem is two-dimensional in the rectangular coordinate system.

II. Formulation

The geometry of the present two-dimensional boundary-value problem is shown in Fig. 1. The transmitting and receiving antennas are located on the surface of the ground. The transmitting antenna emits a pulsed electromagnetic wave into the ground in which

Manuscript received October 17, 1991; revised April 8, 1991. This work was supported by a consortium of 15 oil and service companies and by the Texas Advanced Research Program.

The authors are with the Department of Electrical Engineering, University of Houston, Houston, TX 77204-4793.

IEEE Log Number 9101476.